



Characterizing the role of *Tupaia* DNA damage inducible transcript 3 (*DDIT3*) gene in viral infections

Xiao Zheng^{a,b}, Ling Xu^{b,d,e}, Maosen Ye^{b,c}, Tianle Gu^{b,c}, Yu-Lin Yao^{b,c}, Long-Bao Lv^e, Dandan Yu^{b,c,e,**}, Yong-Gang Yao^{b,c,d,e,*}

^a School of Life Sciences, Division of Life Sciences and Medicine, University of Science and Technology of China, Hefei, Anhui, 230026, China

^b Key Laboratory of Animal Models and Human Disease Mechanisms of the Chinese Academy of Sciences and Yunnan Province, Kunming Institute of Zoology, Chinese Academy of Sciences, Kunming, Yunnan, 650204, China

^c Kunming College of Life Science, University of Chinese Academy of Sciences, Kunming, Yunnan, 650204, China

^d KIZ-CUHK Joint Laboratory of Bioresources and Molecular Research in Common Diseases, Kunming Institute of Zoology, Chinese Academy of Sciences, Kunming, 650204, China

^e National Resource Center for Non-Human Primates, National Research Facility for Phenotypic & Genetic Analysis of Model Animals (Primate Facility), Kunming Institute of Zoology, Chinese Academy of Sciences, Kunming, Yunnan, 650107, China

ARTICLE INFO

Keywords:

Tree shrew
DDIT3
Viral infection
Innate immune response
MAVS

ABSTRACT

DNA damage inducible transcript 3 (DDIT3, also known as CHOP) belongs to the CCAAT/enhancer-binding protein (C/EBP) family and plays an essential role in endoplasmic reticulum stress. Here, we characterized the potential role of the Chinese tree shrew (*Tupaia belangeri chinensis*) DDIT3 (tDDIT3) in viral infections. The tDDIT3 protein is highly conserved and has a species-specific insertion of the SQSS repeat upstream of the C-terminal basic-leucine zipper (bZIP) domain. Phylogenetic analysis of DDIT3 protein sequences of tree shrew and related mammals indicated a closer genetic affinity between tree shrew and primates than between tree shrew and rodents. Three positively selected sites (PSSs: Glu83, Pro93, and Ser172) were identified in tDDIT3 based on the branch-site model. Expression analysis of tDDIT3 showed a constitutively expressed level in different tissues and a significantly increased level in tree shrew cells upon herpes simplex virus type 1 (HSV-1) and Newcastle disease virus (NDV) infections. Overexpression of tDDIT3 significantly increased the production of HSV-1 and vesicular stomatitis virus (VSV) in tree shrew primary renal cells (TSPRCs), whereas tDDIT3 knockout in tree shrew stable cell line (TSR6 cells) had an inhibitory effect on virus production. The enhanced effect on viral infection by tDDIT3 was not associated with the three PSSs. Mechanistically, tDDIT3 overexpression inhibited type I IFN signaling. tDDIT3 interacted with tMAVS through CARD and PRR domains, but not with other immune-related factors such as tMDA5, tSTING and tTBK1. Collectively, our results revealed tDDIT3 as a negative regulator for virus infection.

1. Introduction

The Chinese tree shrew (*Tupaia belangeri chinensis*) was a small mammal widely distributed in the tropical shrubs or forests of South China and proximate regions of South and Southeast Asia (Peng et al., 1991). There are many attempts to use this animal for biomedical researches due to its unique features, such as rat-sized body weight (100–150 g), high brain-to-body mass ratio, relatively short

reproductive cycle (6 weeks) and life span (8–10 years), and low maintenance cost (Xiao et al., 2017; Yao, 2017). In recent years, tree shrew has been used as a valid experimental model in neuroscience research (Fan et al., 2018; Savier et al., 2021), cancer research (Ge et al., 2016; Lu et al., 2021b; Sun et al., 2021), infectious disease studies (Li et al., 2018; Luo et al., 2021; Xu et al., 2020c; Zhang et al., 2019), and other diseases (Che et al., 2021; Chen et al., 2020). Accumulating data showing that tree shrew was susceptible to many human pathogens,

* Corresponding author. Key Laboratory of Animal Models and Human Disease Mechanisms of the Chinese Academy of Sciences and Yunnan Province, Kunming Institute of Zoology, Chinese Academy of Sciences, Kunming, Yunnan, 650204, China..

** Corresponding author. Key Laboratory of Animal Models and Human Disease Mechanisms of the Chinese Academy of Sciences and Yunnan Province, Kunming Institute of Zoology, Chinese Academy of Sciences, Kunming, Yunnan, 650204, China.

E-mail addresses: yudandan@mail.kiz.ac.cn (D. Yu), yaoyg@mail.kiz.ac.cn (Y.-G. Yao).

<https://doi.org/10.1016/j.dci.2021.104307>

Received 16 August 2021; Received in revised form 1 November 2021; Accepted 1 November 2021

Available online 5 November 2021

0145-305X/© 2021 Elsevier Ltd. All rights reserved.

including hepatitis C virus (HCV) (Amako et al., 2010; Xu et al., 2007, 2020c), hepatitis B virus (HBV) (Guo et al., 2018; Kock et al., 2001; Luo and Zheng, 2020), influenza virus (Xu et al., 2019b; Yang et al., 2013), HSV-1 (Li et al., 2016), and severe acute respiratory syndrome coronavirus 2 (SARS-CoV-2) (Xu et al., 2020a). Since the completion and refinement of the Chinese tree shrew genome (Fan et al., 2013, 2019; Ye et al., 2021), we had made great efforts to characterize the innate immune system of this animal, with the aim to learn more about the genetic basis of using tree shrew as an infectious disease model. We characterized the molecular characters and functions of tree shrew RIG-I-like (RLR) receptors (Xu et al., 2016), Toll-like (TLR) receptors (Yu et al., 2016), mitochondrial antiviral signaling protein (MAVS) (Xu et al., 2015), guanylate-binding proteins (GBP) (Gu et al., 2019a), and 2', 5'-oligoadenylate synthetases (OASs) (Yao et al., 2019). For better sharing of the tree shrew resources, we also created two tree shrew cell lines of renal tissue (Gu et al., 2019b) and hepatic tissue origins (Zhang et al., 2020b). Moreover, a comparison of the tree shrew skin structure (Zhang et al., 2020a) and neocortex development (Yin et al., 2020) with other species showed a closer resemblance to primates than to rodents. All these results from our studies of tree shrews, together with the related ones from the field (Lu et al., 2021b; Xiao et al., 2017), undoubtedly suggesting for a promising and bright future for the usage of tree shrew in basic and biomedical researches (Yao, 2017).

DNA damage inducible transcript 3 (DDIT3) is a member of the CCAAT/enhancer-binding protein (C/EBP) family. It was also known as growth arrest and DNA damage inducible gene 153 (GADD153) and C/EBP homologous protein (CHOP) (Oyadomari and Mori, 2004). DDIT3 has been reported to play a pivotal role in the pathogenesis of neurodegenerative disorders (Baleriola et al., 2014; Li et al., 2021; Pennuto et al., 2008) and metabolism dysfunction including type 2 diabetes and hepatic steatosis (Yong et al., 2021) and renal dysfunction (Zhang et al., 2015). Most of these studies linked DDIT3 as a main conduit to endoplasmic reticulum (ER) stress (Yang et al., 2017) or as a transcription regulator to modulate autophagy (Rouschop et al., 2010) and apoptosis (Medigeshi et al., 2007). It was also found that DDIT3 played a role in viral infection (Hu et al., 2018; Wang et al., 2020). As virus was likely to synthesize and modify the viral proteins in ER, it would cause incorrect procession of proteins and triggered the unfolded protein response (UPR), which finally induced the production of DDIT3 (Hu et al., 2018). In our recent transcriptomic analyses for tree shrew primary hepatocytes upon HCV infection, we found that tree shrew *DDIT3* (*tDDIT3*) was upregulated (authors' unpublished data), which was consistent with the report for an increased expression of *DDIT3* upon HCV infection (Ke and Chen, 2011). In addition, an evolutionary analysis for potential positive selection of the *tDDIT3* gene identified several positively selected sites (PSSs) in this gene (see below), that is the reason why we began our work on characterizing the role of *tDDIT3* in viral infection. In this study, we firstly performed an evolutionary analysis and functional characterization of *DDIT3* in the Chinese tree shrews. We found that this gene had a tissue-specific expression pattern. Overexpression of *tDDIT3* inhibited type I interferon signaling activation upon viral infection, and enhanced virus production in tree shrew cells. We also provided suggestive evidence that *tDDIT3* interacted with *tMAVS*.

2. Materials and methods

2.1. Experimental animals and cells

This study is a part of our previous and ongoing projects that aim to characterize the genetic features of the tree shrew immune system (Gu et al., 2019a; Xu et al., 2015, 2016, 2020c; Yao et al., 2019, 2020; Yu et al., 2014, 2016). We used tree shrew tissues, including heart, liver, spleen, lung, kidney, small intestine and brain that were collected in these previous studies. Briefly, tissues were collected from adult tree shrews from the experimental animal core facility of the Kunming Institute of Zoology (KIZ) after lethally anesthetized by pentobarbital,

and were immediately frozen in liquid nitrogen and were stored at -80°C . The experimental protocol was approved by the Institutional Animal Care and Use Committee of KIZ. We followed the same procedure in our previous studies (Xu et al., 2016; Yu et al., 2014) to isolate and culture tree shrew primary renal cells (TSPRCs). TSR6 (tree shrew renal cell #6) was established in our previous study (Gu et al., 2019b), and HEK293T cell line was introduced from the Kunming Cell Bank of KIZ. All cells were cultured in high-glucose Dulbecco's modified Eagles medium (DMEM; Gibco-BRL, USA) supplemented with 10% fetal bovine serum (FBS; Gibco-BRL, USA) and 1% penicillin/streptomycin (Gibco-BRL, USA) in a humidified incubator at 37°C in 5% CO_2 .

2.2. Total RNA extraction and quantification

Total RNAs were extracted from tree shrew tissues and cells by using the RNA simple Total RNA Kit (TIANGEN, Beijing) according to the manufacturer's instruction. We used these RNA samples with an A260/A280 ratio of 1.8–2.0 for the subsequent quantification. Briefly, around 2 μg of total RNA was used to synthesize complementary DNA (cDNA) by using oligo-dT18 primer, random primer and M-MLV reverse transcriptase (Promega, USA). Quantitative real-time PCR (qRT-PCR) was performed in a total volume of 20 μL reaction system, which contains 10 μL of $2 \times$ SYBR green Premix Ex Taq IiiTaq, 0.4 μM (around 1 μL) gene-specific primer pair (Table S1), 1 μL of cDNA, and 8 μL of ddH_2O . The qRT-PCR was performed on a MyIQ2 Two-Color Real-Time PCR Detection system (Bio-Rad, USA), as described in our previous studies (Gu et al., 2019a; Xu et al., 2015; Yao et al., 2019; Yu et al., 2014) with the following conditions: one denaturation cycle at 95°C for 1 min, 40 amplification cycles of 95°C for 15 s and 55°C for 15 s. The PCR product of respective gene was serially diluted, and the 10^{-3} - 10^{-10} dilutions were used for making the standard curve for quantification of the target gene. The Ct values were measured relative to the corresponding standard curve. Tree shrew house-keeping gene *β -actin* was used for the normalization of the target gene.

2.3. Evolutionary analyses of the *DDIT3* gene

We retrieved the DDIT3 protein sequences of 12 mammalian species from the ENSEMBL (<http://www.ensembl.org/index.html>) (Table S2) and aligned these sequences by the Clustal W method of MEGA7.0 (Kumar et al., 2016). The neighbor-joining (NJ) method was used to construct a phylogenetic tree, with 1000 bootstrap replications. We tested potentially selective pressure acting on protein-coding genes by estimating the ratio of non-synonymous to synonymous substitutions ($\omega = \text{dN/dS}$) between the coding parts of homologs, with $\omega = 1$ meaning neutral mutations and $\omega > 1$ for positive selection. We followed the same procedure in our previous study (Fan et al., 2018) to perform a positive selection test by the branch-site model (Yang and Nielsen, 2002; Zhang et al., 2005), and the codeml software implemented in PAML4 (Yang, 2007) package was used. The likelihood of positive selection (tree shrew branch as the fixed foreground branch, $\omega_2 = 1$) was compared to the likelihood under the null hypothesis (non-fixed foreground branch) by using likelihood ratio test, to test whether a proportion of sites in the sequence provides statistically significant support for $\omega > 1$ in the foreground branch. Individual codon sites putatively under positive selection were identified using the site-specific Bayes Empirical Bayes (BEB) method (Yang et al., 2005), with each codon site being assigned with a corresponding posterior probability.

2.4. Plasmid construction

Based on the *tDDIT3* gene information from the treeshrewDB database (<http://www.treeshrewdb.org/>) (Fan et al., 2019), we designed specific primer pairs (Table S1) to amplify the open reading frame of *tDDIT3* and cloned it into FLAG-tagged pCMV-3Tag-8 (Stratagene, USA) with *Bam*H I and *Xho* I. We made three *tDDIT3* mutants by using the

multisite-directed mutagenesis (StrataGene, USA) as described in our previous studies (Gu et al., 2021; Xu et al., 2020c), and each mutant contains one PSS as identified in the above evolutionary analysis. These tDDIT3 mutants p.E83D, p.S89_S92 del (the 93rd residue underwent positive selection due to the inserted SQSS repeat, so we created this variant by deleting the SQSS repeat), and p.S172A. Expression vector for tTRIM25 was generated using specific primers and was cloned into pCMV-3Tag-8 vector (Table S1). Ub-HA vector was a kind gift from Bingyu Mao's laboratory at KIZ. All plasmids were confirmed by sequencing.

2.5. Virus infection

Herpes simplex virus type 1 strain 17+ (HSV-1), HSV-1 with a GFP tag (HSV-1-GFP), vesicular stomatitis virus tagged by GFP (VSV-GFP, Indiana strain), and Newcastle disease virus (NDV) were lentogenic strain LaSota taken from our previous study (Gu et al., 2021; Xu et al., 2016). HSV-1 was amplified as in our previous studies (Xu et al., 2016, 2020b). For viral infection, TSPRCs or TSR6 were seeded in 12-well plates (1×10^5 cells per well) for growth overnight, then were washed with serum-free DMEM twice. Cells were incubated with HSV-1 (multiplicity of infection [MOI] = 1), VSV (MOI = 0.01), NDV (MOI = 1) for 1 h in serum-free DMEM, followed by culture in fresh growth medium containing 10% FBS until harvest at the indicated time for quantification of mRNA or protein level of the target gene. The production of VSV-GFP and HSV-1-GFP in infected cells was quantified by using flow cytometry as described in our previous study (Xu et al., 2020b).

2.6. Western blotting

Different tree shrew tissues (heart, liver, spleen, lung, kidney, brain, small intestine), were lysated by using the protein lysis buffer (Beyotime, Shanghai). The tree shrew cells were seeded in a 6-well plate at a density of 4×10^5 cells per well for growth overnight, then were transfected with the respective vectors using Lipofectamine™ 3000 (Thermo Fisher, USA). The transfected cells were harvested in RIPA lysis buffer (Beyotime, Shanghai) on ice, and the lysate supernatant were obtained by centrifuging at 12,000 g for 10 min at 4 °C. Around 30 µg of proteins were separated by 12% SDS-PAGE gel and transferred into polyvinylidene fluoride membranes (Bio-Rad, USA) using standard procedures described in our previous studies (Xu et al., 2020b; Yao et al., 2020). The membranes were blocked with 5% nonfat dry milk in Tris-buffered saline containing 0.1% Tween 20 (TBST) at room temperature for 2 h. Then, specific primary antibody was used to probe the respective protein overnight at 4 °C. We used the following primary antibodies for Western blot: mouse anti-DDIT3 (1:1000; Cat# 66741-1-Ig, Proteintech), mouse anti-FLAG (1:5000; Cat# T20008, Abmart), mouse anti-Myc (1:5000; Cat# MA121316, Thermo), rabbit anti-HA (1:5000; Cat# 3724S, CST), mouse anti-β-actin (1:10000; Cat# E1C602-2, Enogene), mouse anti-GAPDH (1:10000; Cat# E12-052-4, EnoGene), mouse anti-ubiquitin (1:1000; Cat# sc-8017, Santa Cruz). Membranes were washed three times with $1 \times$ TBST (each 5 min) and were incubated with anti-mouse (Cat# 474-1806, 1:10,000, KPL, USA) or anti-rabbit (Cat# 074-1506, 1:10,000, KPL, USA) secondary antibody for 1 h at room temperature before being visualized by using the enhanced chemiluminescence (ECL) reagents (Millipore). ImageJ software was used to compare the densitometry of bands.

2.7. Generation of a tDDIT3 knockout cell line

We knocked out the tDDIT3 gene in TSR6 cell line (TSR6-DDIT3-KO cell line) by using the CRISPR-Cas9 system (Ma et al., 2018; Ran et al., 2013), as described in our previous studies (Gu et al., 2019a). In brief, the sgRNAs (tDDIT3-sgRNA-F, 5'-CACCGCCAGCTGGA-CAGTGTCCCGA-3'/tDDIT3-sgRNA-R, 5'-AAACTCGGGACACTGTCCAGCTGGC-3'), targeting the open reading

frame of tDDIT3, were designed by the CRISPR Design Tool (<http://bioinfo.gp.cnb.csic.es/tools/breakingcas/index.php>) (Oliveros et al., 2016). The sgRNAs were annealed and cloned into the pX330-T7 vector expressing mCherry, then the construct was transfected into TSR6 cells. After transfection for 48 h, transfected cells expressing mCherry were sorted by flow cytometry for growth to achieve the stable lines. Genomic DNA of TSR6 cells with potential tDDIT3 knockout was extracted by AxyPrep Multisource Genomic DNA Miniprep Kit (Axygen, USA), and was genotyped by using primer pair tDDIT3-sgF, 5'-TTTAAACGG-CAGGACAG-3'/tDDIT3-sgR, 5'-AGATTCCAGTCAGAGCTC-3'. We obtained a stable cell clone with a frame shift mutation (c.33del_G) that disrupts the open reading frame of tDDIT3.

2.8. Luciferase reporter assay

HEK293T cells were seeded in 24-well plates at a density of 5×10^4 cells per well for an overnight culture. Cells were transfected with 100 ng of luciferase reporter vector (IFN-β-Luc [a kind gift from Bin Li, Institute Pasteur of Shanghai, CAS], NF-κB-Luc [Cat# 631912, pNFκB-TA-Luc; Clontech Laboratories], or ISRE-Luc [Cat# 219092, ISRE cis-reporter; Stratagene]; all with human promoter insert), 10 ng of pRL-TK-Renilla (Cat# E2241, Promega; as an internal control), together with a combination of an increased amount (0 ng, 150 ng, 300 ng, and 600 ng) of tDDIT3 expression vector (with empty vector to reach a total amount of 600 ng; Table S1) and one of the reported expression vectors (tMDA5, tMAVS, tSTING and tTBK1) in our previous studies (Xu et al., 2020b, 2020c; Yao et al., 2020) by using Lipofectamine™ 3000 (Thermo Fisher, USA). Dual-Luciferase Reporter Assay System (Promega, USA) was used for measuring luciferase activity on an infinite M1000 Pro multimode microplate reader (Tecan, Switzerland). We also performed a luciferase assay for the tree shrew IFN-β-Luc from our previous study (Xu et al., 2015, 2020b) using the same procedure for human IFN-β-Luc.

2.9. Immunoprecipitation assay

The HEK293T cells were seeded in a 10-cm cell culture dish (1×10^7 cells per dish) and cultured overnight, then were transfected with indicated expression vectors (total 10 µg) for 36 h. Cells were harvested and lysed in RIPA lysis buffer on ice for 1 h, followed by a centrifuge at 12,000 g for 10 min at 4 °C to collect lysate supernatant. Protein G agarose beads (Life Technologies, USA) were incubated with indicated antibodies for 2 h at room temperature to form the antibody-bead complex, and incubated with the cell lysate supernatant overnight at 4 °C. After four washes with the RIPA lysis buffer, the immunoprecipitates were resuspended in loading sample buffer for Western blotting.

2.10. Statistical analysis

Comparisons of the relative mRNA and protein levels of tDDIT3 in different tissues were conducted by one-way ANOVA with the Tukey's post-hoc test. The unpaired Student's *t*-test was performed to measure the difference between two groups by using GraphPad Software (La Jolla, CA, USA). Data were presented as mean ± SD. A *P* value < 0.05 was considered to be statistically significant.

3. Results

3.1. Evolutionary analysis of tDDIT3

The open reading frame of tDDIT3 is 519 bp (GenBank accession number OK076936), which encodes a putative polypeptide of 172 residues. We aligned the tDDIT3 protein sequence with those of 11 mammalian species to discern overall sequence identity and conserved domains. The tDDIT3 has a high sequence identity with the DDIT3 from other species, and has a species-specific insert of the Serine-Glutamine-Serine-Serine (SQSS) repeat (Fig. S1). A conserved DNA binding domain,

basic leucine zipper (bZIP) (Ron and Habener, 1992; Ubeda et al., 1996), was identified at the C-terminal of the tDDIT3 protein (Fig. S1).

To further define the evolutionary relationship of tDDIT3 with those of the other mammals, a phylogenetic tree was constructed using NJ method based on the DDIT3 protein sequence alignment (Fig. S1). Tree shrew formed a clade with primates (Fig. 1A), which is consistent with our previous report showing a close genetic affinity of tree shrew to primates (Fan et al., 2013). We performed branch-site model (Yang and Nielsen, 2002) to discern potential selective pressure on tDDIT3 and identified three PSSs (Fig. 1B). The first PSS was located in the 83rd position (the numbering refers to the aligned DDIT3 protein sequences in Fig. S1), which is a glutamic acid (E) in tree shrew but an aspartic acid (D) in other mammals. Another PSS was located in the 93rd position, which is close to the tree shrew unique SQSS insertion. Both the 83rd and the 93rd sites were located in the N-terminal of tDDIT3, which was said to be responsible for transcriptional activation/repression and affected the transcriptional activity of tDDIT3 (Ubeda et al., 1996). The third PSS was located in the 172nd position of tDDIT3, in which tree shrew has a serine (S), but other mammals have an alanine (A). The 172nd residue was located in the C-terminal which contained a basic region mediating sequence-specific DNA binding along with a leucine zipper motif for dimerization (Tsukada et al., 2011). Based on the predicted structure and domains of DDIT3, the three PSSs of tDDIT3 might affect its function.

3.2. Tissue expression pattern of tDDIT3 in healthy tree shrews

We next determined the tissue expression pattern of tDDIT3 in the Chinese tree shrews. Measurement of tDDIT3 mRNA levels in the heart, liver, spleen, lung, kidney, small intestine and brain tissues showed that the brain has a relatively high mRNA level, followed by the lung, whereas the small intestine has the lowest tDDIT3 mRNA level (Fig. 1C). Western blot result for tDDIT3 protein revealed an overall similar

expression pattern with that of mRNA expression, with the highest protein level in the brain tissue (Fig. 1D). The different tissue expression pattern of tDDIT3 might be associated with its functional diversity in different tissues.

3.3. tDDIT3 was upregulated by virus infections

We determined the alteration of tDDIT3 mRNA levels in cultured TSPRCs upon NDV and HSV-1 infection. Along with the increased mRNA expression level of tIFNB1 in TSPRCs in response to viral infections (Fig. 1E, left panel), we observed a relatively late induction of tDDIT3 mRNA expression that was significantly upregulated at 12 h (Fig. 1E, right panel) and later time points (Fig. S2). Our observation for an upregulated tDDIT3 mRNA in virus-infected tree shrew cells was consistent with these previous reports for an induced DDIT3 expression in Madin-Darby bovine kidney cells with bovine viral diarrhea virus infection (Wang et al., 2020) and in Huh 7 cells with HCV infection (Ke and Chen, 2011). Collectively, these findings indicated that tDDIT3 may be involved in modulating virus infections.

3.4. tDDIT3 promoted virus production

To examine the potential effect of the upregulated tDDIT3 expression during the viral infection, and to answer whether the three PSSs in tDDIT3 would have an effect on virus production, we firstly transfected the expression vectors of wild-type tDDIT3 (tDDIT3-WT) and three mutants carrying the PSSs (p.E83D, p.S89_S92 del, and p.S172A) in TSPRCs. Transfected cells were then subjected to VSV-GFP infection for 12 h and HSV-1-GFP infection for 48 h, respectively. Flow cytometry results showed that overexpression of tDDIT3-WT or its mutants all enhanced the production of GFP-tagged VSV and HSV-1, as indicated by the increased level of GFP expression compared to that of the control cells transfected with empty vector (Fig. 2). Consistent with our previous

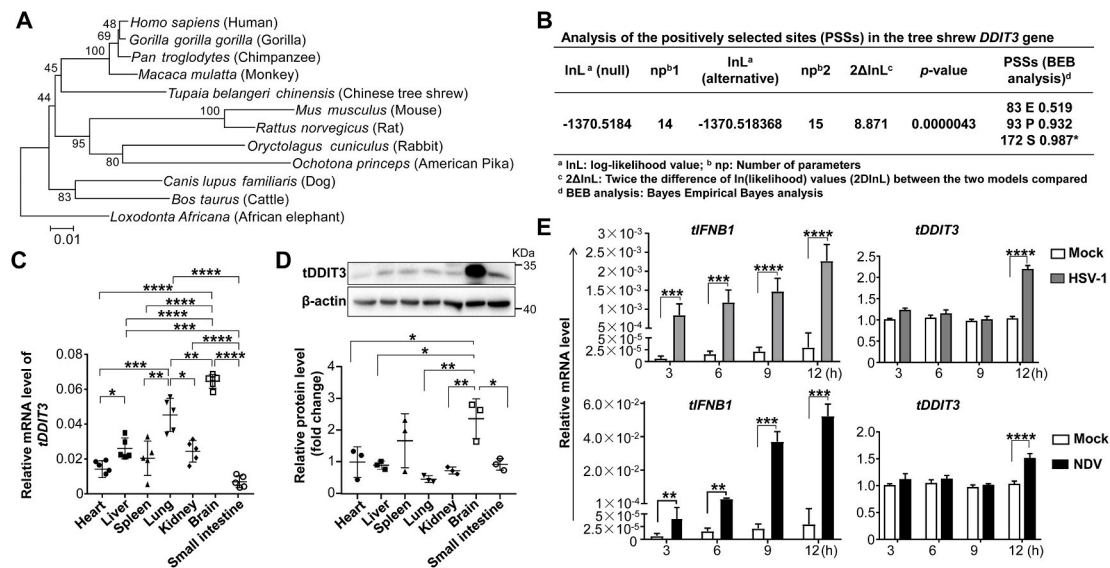


Fig. 1. Evolutionary analysis of tree shrew DDIT3 and expression of this gene in tree shrew tissues and cells. (A) Neighbor-joining tree based on the DDIT3 protein sequences, with *Loxodonta Africana* as the outgroup. The values on the branches refer to the support of 1000 bootstrap replications. Sequence information for each species was listed in Table S2 (B) Positive selection analysis of the tree shrew DDIT3 gene. (C) Relative mRNA levels of tDDIT3 in different tree shrew tissues (n = 5 animals). The tDDIT3 mRNA level was detected by qRT-PCR and normalized to β-actin. Values of relative mRNA level were presented as mean ± SD. (D) Immunoblot of endogenous tDDIT3 in seven tissues of the tree shrew. Densitometry analysis for the tDDIT3 protein level was performed using ImageJ software, with normalization to β-actin. Values of the relative protein level were presented as mean ± SD. Group differences in (C–D) were analyzed by one-way ANOVA with the Tukey's post-hoc test, *P < 0.05, **P < 0.01, ***P < 0.001, ****P < 0.0001. (E) Increased mRNA levels of tDDIT3 in tree shrew primary renal cells (TSPRCs) upon viral infection. TSPRCs (5 × 10⁴ cells) were grown in 24-well plates and infected with HSV-1 (MOI = 1) (upper) or with NDV (MOI = 1) (lower) at the indicated times. The mRNA levels of tIFNB1 (left) and tDDIT3 (right) were detected by qRT-PCR and normalized to β-actin. The data in (E) were representative of three independent experiments. Values of relative mRNA level in (E) were presented as mean ± SD. *P < 0.05, **P < 0.01, ***P < 0.001, ****P < 0.0001, two-tailed unpaired Student's t-test.

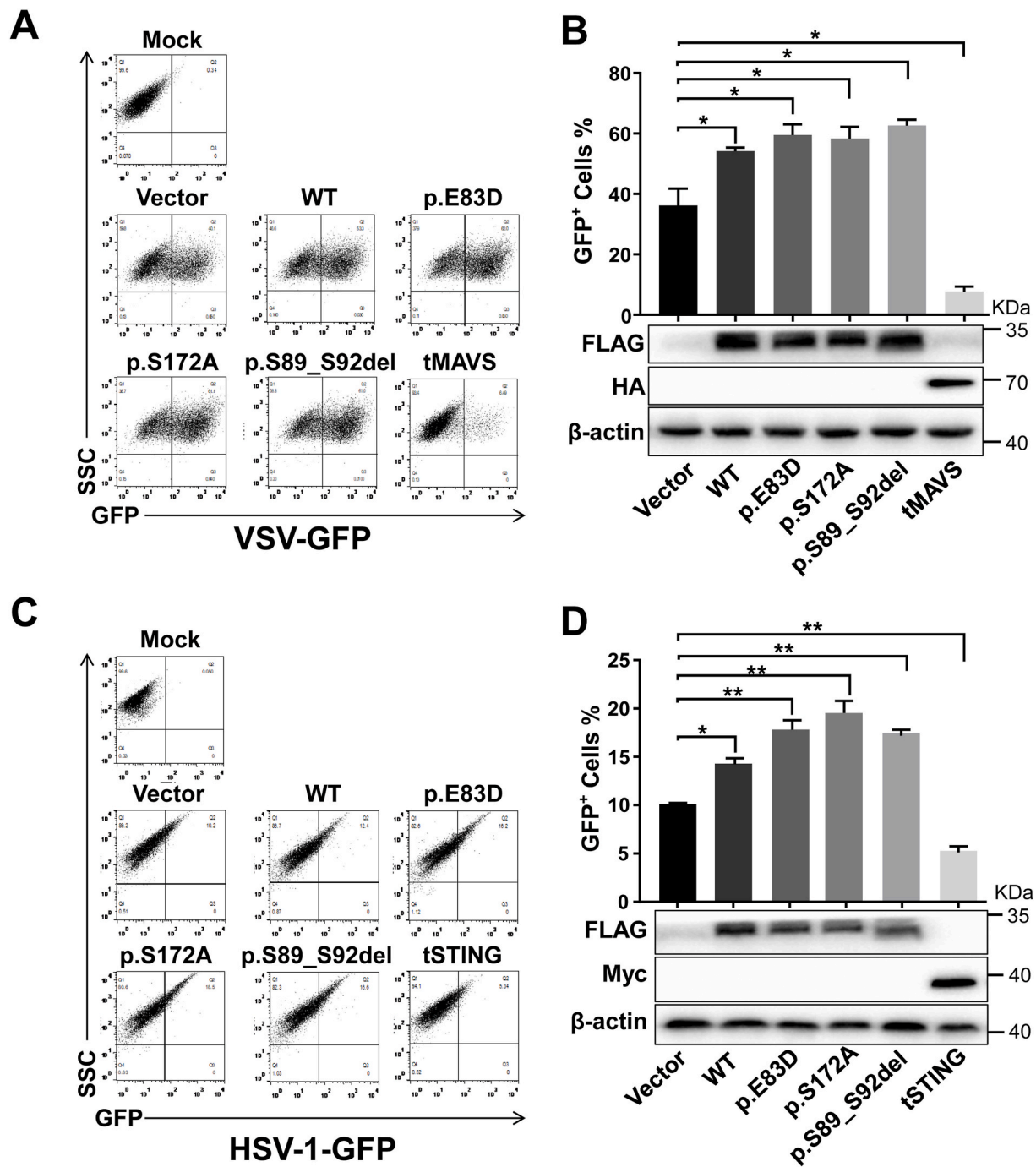


Fig. 2. Overexpression tDDIT3 increased viral infection in TSPRCs. Flow cytometry analysis and quantification of virus production in TSPRCs overexpressing the indicated expression vectors upon GFP-tagged VSV (VSV-GFP, A and B) infection and HSV-1 (HSV-1-GFP, C and D) infections. TSPRCs were seeded in 12-well plates and transfected with empty vector (Vector), expression vectors for wild-type tDDIT3 (WT) and the three mutants with the PSSs (p.E83D, p.S89_S92 del, and p.S172A) for 24 h, respectively, before VSV-GFP infection (MOI = 0.01) for 12 h and HSV-1-GFP infection (MOI = 1) for 48 h. Overexpression of tMAVS and tSTING was used as a positive control for anti-RNA virus and anti-DNA virus infection, respectively. Successful overexpression of the indicated expression vector was detected by Western blot and was listed below the bar graphs of (B) and (D). Percentages of GFP positive cells (GFP⁺ cells) were quantified using flow cytometry. The data were representative of three independent experiments. Values were presented as mean ± SD. **P* < 0.05, ***P* < 0.01, two-tailed unpaired Student's *t*-test.

studies, overexpression of tSTING (Xu et al., 2020b) and tMAVS (Xu et al., 2015) as positive controls, suppressed the virus production. We did not observe any apparent differences regarding the enhancing effect on virus production between WT tDDIT3 and each of the three tDDIT3 mutants with PSSs (Fig. 2). These results suggested that the three PSSs might be irrelevant to tDDIT3's role in modulating viral infection.

To further confirm the enhancing effect of tDDIT3 on viral infections, we generated tDDIT3-deficient cells (TSR6-tDDIT3-KO cells) using the

CRISPR/Cas9 method in the TSR6 cell line (Gu et al., 2019b). We would expect that knockout of endogenous tDDIT3 inhibits virus production. We obtained a mutant TSR6 cell line with a deletion c.33del_G (Fig. 3A) that eliminated the tDDIT3 protein expression (Fig. 3B). As expected, the production of GFP-tagged VSV (Fig. 3C–D) and HSV-1 (Fig. 3E–F) were significantly reduced in TSR6-tDDIT3-KO cells relative to WT cells, with a comparable effect to the overexpression of tSTING and tMAVS in the WT cells. These results indicated that endogenous tDDIT3 has an

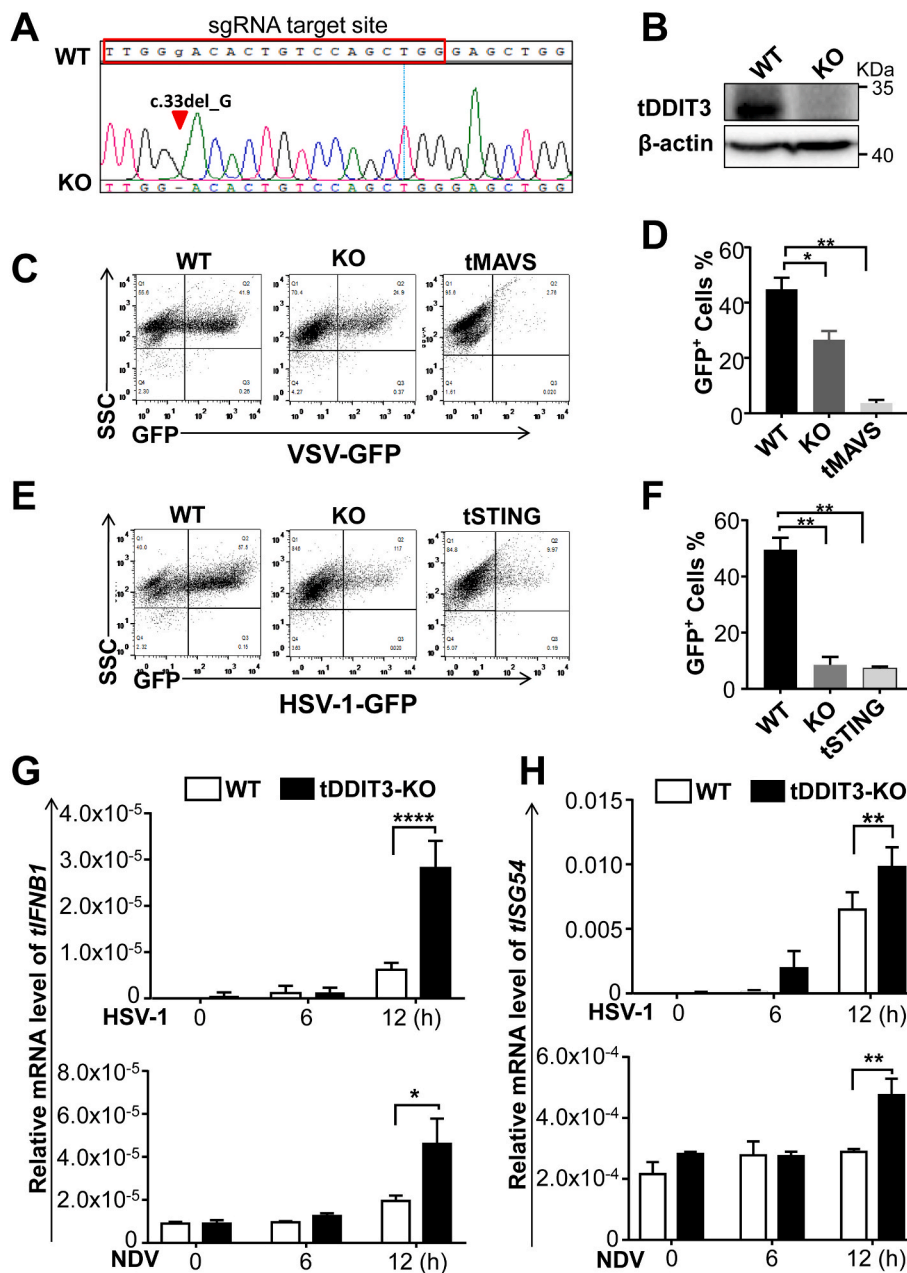


Fig. 3. Knockout of tDDIT3 inhibited virus production in TSR6 cells. (A) Sequencing chromatograph showing an introduced deletion in TSR6 cells (TSR6-tDDIT3-KO, KO) by gene editing. The sgRNA target site was marked in a box on the wild type (WT) sequence. (B) Western blot showing a lack of endogenous tDDIT3 in TSR6-tDDIT3-KO cells relative to TSR6 WT cell. (C–F) Reduced virus production of GFP-tagged VSV (VSV-GFP, C and D) and HSV-1 (HSV-1-GFP, E and F) was observed in TSR6-tDDIT3-KO cells. Percentage of GFP positive cells (GFP⁺ cells) were quantified using flow cytometry. (G–H) Upregulation of mRNA expression levels of *tIFN1* and *tISG54* in TSR6-tDDIT3-KO cells and WT cells upon virus infection. The procedure for HSV-1 (upper) and NDV (lower) infections and quantification of the mRNA levels of *tIFN1* (left) and *tISG54* (right) were same to Fig. 1E. The data were representative of three independent experiments. Values were presented as mean \pm SD. * $P < 0.05$, ** $P < 0.01$, *** $P < 0.0001$, two-tailed unpaired Student's *t*-test.

enhanced effect on virus production.

3.5. tDDIT3 inhibited type I IFN signaling

To determine whether tDDIT3 suppressed antiviral innate immune response via the type I interferon (IFN) signaling, we measured the mRNA expression levels of IFN-stimulated genes *tIFN1* and *tISG54* in TSR6-tDDIT3-KO cells infected with HSV-1 and NDV. Deficiency of tDDIT3 could significantly increase the mRNA expression of *tIFN1* (Fig. 3G) and *tISG54* (Fig. 3H) upon HSV-1 and NDV infections for 12 h, suggesting that tDDIT3 affected type I IFN signaling.

Next, we attempted to identify the potential target of tDDIT3 to quench the innate immune response by co-expressing these cellular adaptor proteins, sensors or mediators of antiviral signaling (e.g. tMDA5, tMAVS, tSTING and tTBK1) with tDDIT3 in HEK293T. Cells were co-transfected with expression vector for tMDA5, tMAVS, tSTING or tTBK1, together with an increased amount of tDDIT3 expression vector (Fig. 4A). We found that overexpression of tDDIT3 could decrease

IFN- β -Luc, NF- κ B-Luc, ISRE-Luc reporter activities induced by tMDA5, tMAVS, tSTING and tTBK1 overexpression, in a dose-dependent manner, albeit tMDA5 had a relatively lower induction effect compared with tMAVS, tSTING or tTBK1 (Fig. 4B). We observed a similar suppression effect of tDDIT3 on induced tree shrew IFN- β -Luc (tIFN- β -Luc) (Xu et al., 2015) luciferase activity (Fig. S3). Consistent with the similar enhancing effect of tDDIT3 WT and its mutants with the PSSs on virus production (Fig. 2), the three tDDIT3 mutants had an almost equal ability to decrease the IFN- β -Luc reporter activities induced by tMAVS (Fig. 4C).

We further examined the effect of tDDIT3 overexpression on inhibiting type I IFN signaling that was activated by overexpression of tMAVS, tSTING, tMDA5 or tTBK1 in TSPRCs. Co-expression of tDDIT3 and tMAVS, tDDIT3 and tSTING, or tDDIT3 and tTBK1, but not tDDIT3 and tMDA5, significantly reduced the transcription of *tIFN1* (Fig. 4D). This observation was compatible with an explanation that tDDIT3 might affect the antiviral innate immune signaling. Taken together, our results indicated that tDDIT3 negatively regulated type I IFN signaling.

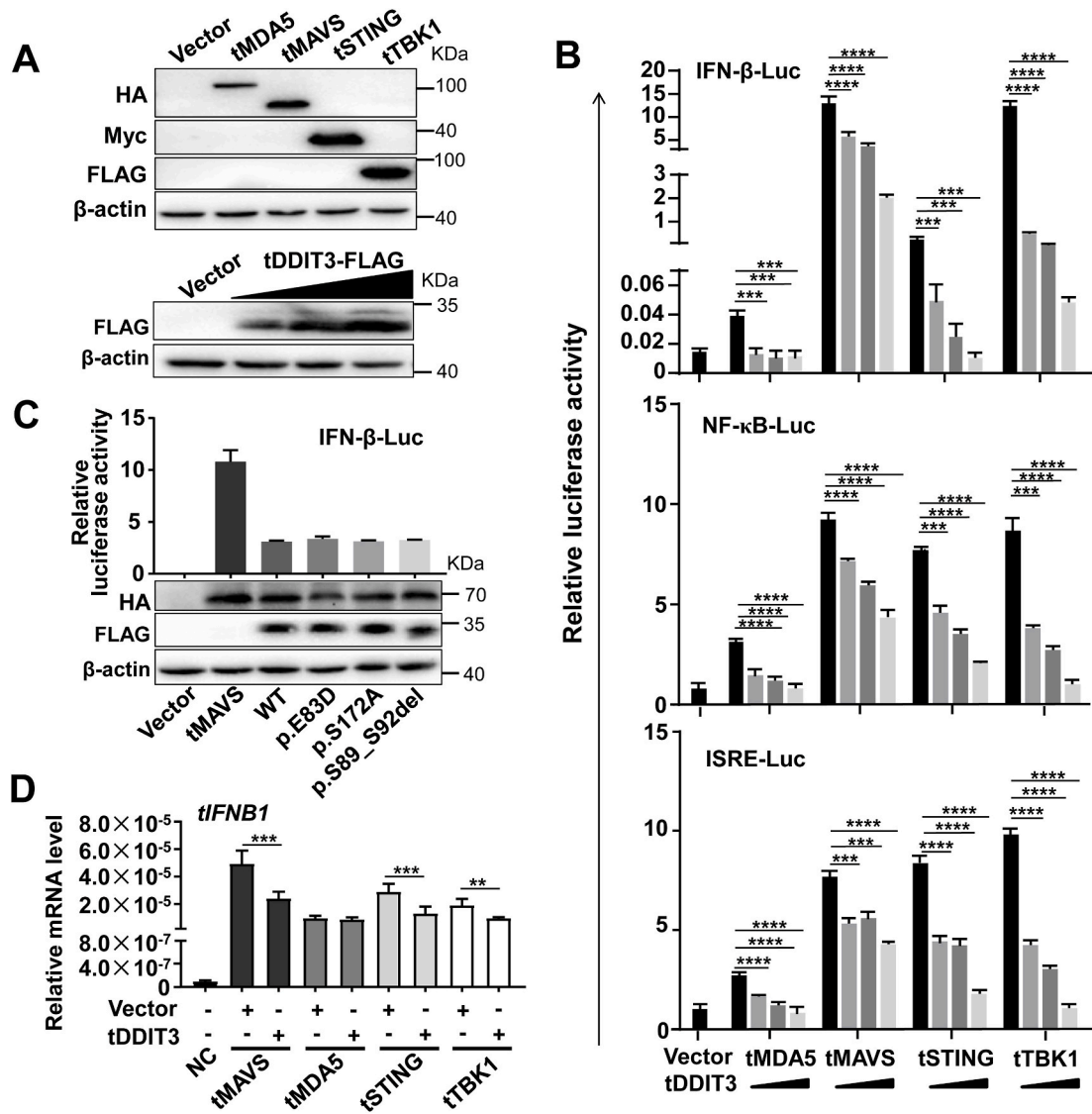


Fig. 4. tDDIT3 suppressed the activation of type I IFN signaling stimulated by overexpression of tMDA5, tMAVS, tSTING and tTBK1. (A) Successful overexpression of the indicated expression vectors in HEK293T cells. Cells were seed in 24-well plates (5×10^4 cells) and grew overnight, followed by transfection with empty vector, expression vector for tMDA5-HA, tMAVS-HA, tSTING-Myc, or tTBK1-FLAG (each 300 ng), and an increased amount (0 ng, 150 ng, 300 ng, and 600 ng) of expression vector for tDDIT3-FLAG. After transfection for 36 h, cells were harvested for Western blot. (B) Overexpression of tDDIT3 reduced IFN- β -Luc, NF- κ B-Luc, ISRE-Luc reporter activities stimulated by overexpressed tMDA5, tMAVS, tSTING and tTBK1 in a dose-dependent manner. HEK293T cells were transfected with the same amount of indicated vectors as in (A), together with indicated luciferase reporter vector (IFN- β -Luc, NF- κ B-Luc, or ISRE-Luc reporter vector; each 100 ng) and TK (10 ng, as an inner control). (C) Wild-type tDDIT3 and its mutants with the three PSSs decreased the IFN- β -Luc reporter activated by overexpressing tMAVS. HEK293T (5×10^4 cells) were transfected with empty vector (Vector, 300 ng) or tMAVS expression vector (300 ng), together with expression vector of wild-type tDDIT3 (WT) or its mutant (p.E83D, p.S89_S92 del, or p.S172A) (each expression vector 150 ng), IFN- β -Luc reporter vector (100 ng), and TK (10 ng, as an inner control). Luciferase assays in (B–C) were performed in cell lysates at 36 h after transfection. (D) tDDIT3 overexpression inhibited the mRNA expression of *IFNB1*. TSPRCs (5×10^4 cells) were transfected with a combination of the indicated expression vector of immune sensor (tMAVS, tMDA5, tSTING, and tTBK1; each 250 ng) and tDDIT3 expression vector (250 ng) or empty vector (250 ng). Cells with transfection or without any transfection (NC) were harvested at 36 h for quantification of *IFNB1* mRNA level by using qRT-PCR. The data were representative of three independent experiments. Values were presented as mean \pm SD. ** $P < 0.01$, *** $P < 0.001$, **** $P < 0.0001$, two-tailed unpaired Student's *t*-test.

3.6. tDDIT3 interacted with tMAVS via its CARD and PRR domains

As overexpression of tDDIT3 decreased IFN- β -Luc, NF- κ B-Luc, ISRE-Luc reporter activities induced by overexpression of tMDA5, tMAVS, tSTING or tTBK1 (Fig. 4B), we performed an immunoprecipitation assay in HEK293T cells to address whether tDDIT3 would physically interact with tMDA5, tMAVS, tSTING or tTBK1. We found that tDDIT3 could bind to tMAVS (Fig. 5A), but not tMDA5 (Fig. 5B), tSTING (Fig. 5C) and tTBK1 (Fig. 5D). To map the domains of tMAVS that mediated the interaction between tDDIT3 and tMAVS, we used three truncated mutants of tMAVS, namely N-terminal caspase recruit domain (CARD), the

middle proline-rich domain (PRR), and C-terminal transmembrane domain (TM) that were generated in our previous study (Yao et al., 2020). Immunoprecipitation assays showed that tDDIT3 could interact with tMAVS-CARD and tMAVS-PRR, but not with tMAVS-TM (Fig. 5E). This result suggested that the CARD and PRR domains of tMAVS might be responsible for the interaction between tMAVS and tDDIT3.

Considering the fact that tDDIT3 overexpression inhibited the type I IFN signaling (Fig. 4), and ubiquitin of both host and pathogen proteins would affect the IFN signaling (Gack et al., 2007; Versteeg et al., 2013; Zheng and Gao, 2020), we performed an assay to show whether the binding of tDDIT3 to tMAVS would enhance the ubiquitin of tMAVS. As

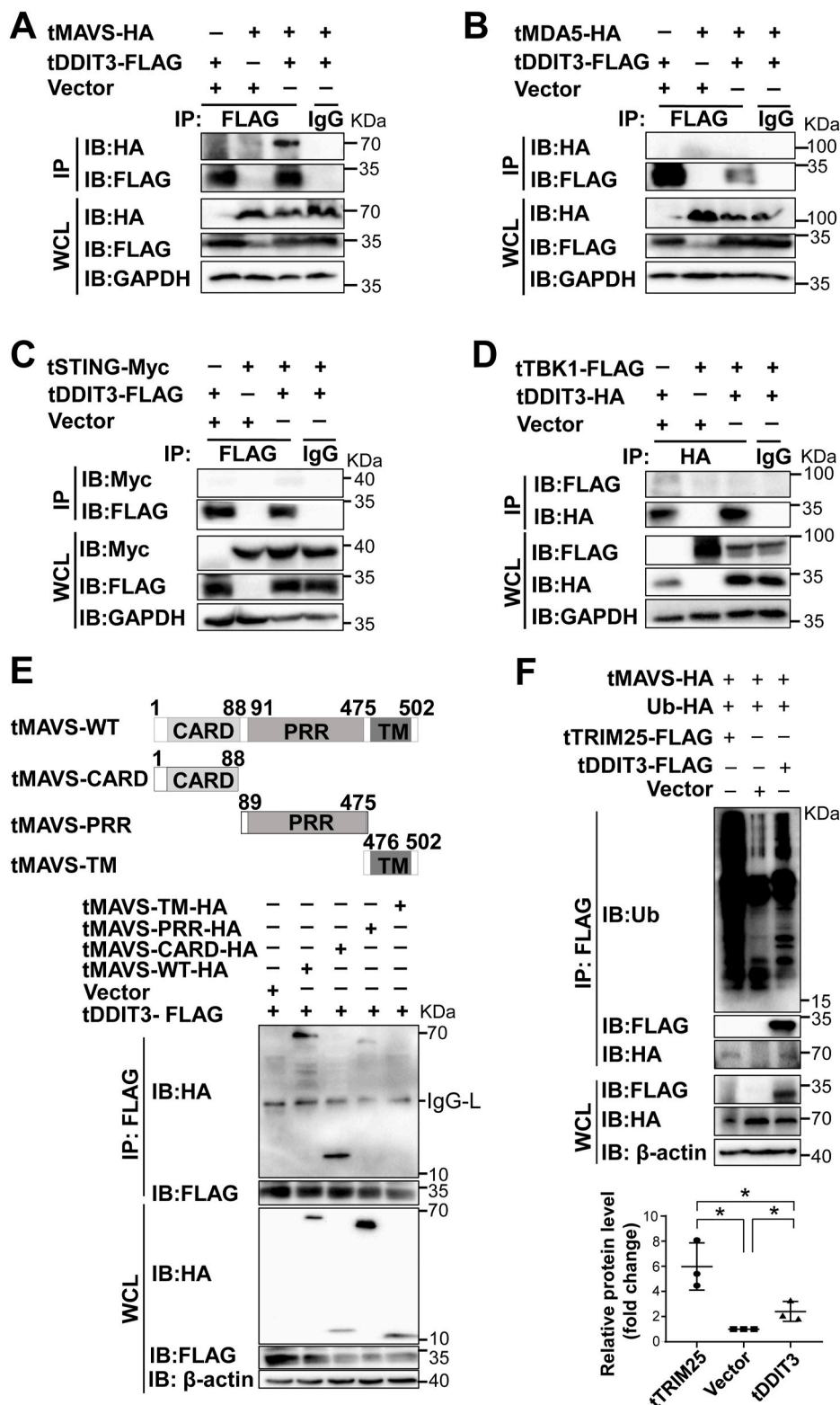


Fig. 5. tDDIT3 interacted with tMAVS via CARD and PRR domain. (A–D) tDDIT3 binds to tMAVS (A), but not tMDA5 (B), tSTING (C) or tTBK1 (D). (E) The CARD and PRR domains of tMAVS bind to tDDIT3. HEK293T (1×10^7 cells) were seeded in 10-cm dish and co-transfected with tDDIT3-FLAG and the indicated expression vector (tMDA5-HA, full-length tMAVS-HA, truncated tMAVS-HA, tSTING-Myc, or tTBK1-FLAG; each 5 μ g) for 36 h before the harvest for immunoprecipitation (IP) analysis. IgG was used as a control. An empty vector served as a negative control. IP assay was performed by using the anti-FLAG antibody. (F) Overexpression of tDDIT3 enhanced the ubiquitination of tMAVS. (Upper) Representative Western blot of anti-FLAG IP; (Lower) Quantification of the relative levels of ubiquitinated tMAVS. HEK293T (1×10^7 cells) were seeded in 10-cm dish for overnight growth, followed by co-transfection of a combination of expression vectors of tMAVS (tMAVS-HA) and ubiquitin (Ub-HA), together with empty vector, tDDIT3-FLAG, or tTRIM25-FLAG (each vector 3 μ g). Overexpression of tTRIM25-FLAG was used as a positive control. Cells were harvested for IP analysis at 36 h after transfection. WCL, whole cell lysate. Mouse anti-ubiquitin antibody was used to probe ubiquitinated tMAVS. We used anti-HA and anti-FLAG antibodies to probe tMAVS and tDDIT3, respectively. The β -actin was used as the loading control. Bars presented as mean \pm SD of the three experiments. * $P < 0.05$, two-tailed unpaired Student's t -test.

shown in Fig. 5F, we found that co-expression of tDDIT3 and tMAVS affected the ubiquitin of tMAVS, but this effect was inferior to that of the co-expression of tTRIM25 and tMAVS, which was included as a positive control (Gack et al., 2007; Versteeg et al., 2013) in the assay. Collectively, our results indicated that interact between tDDIT3 and tMAVS affected the ubiquitin of tMAVS, which might account for the inhibiting effect of DDIT3 on tMAVS-induced type I IFN signaling activation.

4. Discussion

The DDIT3 was firstly characterized as a DNA damage-inducible transcript in mammalian cells upon ultraviolet irradiation and methyl methane sulfonate treatment (Fornace et al., 1988). It played a regulatory role in cell proliferation, metabolism and differentiation (Hu et al., 2018). The DDIT3 was also recognized as a transcription regulator to

modulate autophagy (Ke and Chen, 2011; Rouschop et al., 2010) and apoptosis (Medigeshi et al., 2007) mediated by endoplasmic reticulum stress (Oyadomari and Mori, 2004). In normal physiological condition, *DDIT3* was expressed at an extremely low level, but its expression was greatly increased in some pathological conditions or in response to microbial infections (Hu et al., 2018; Ron and Habener, 1992). There were several reports showing that *DDIT3* modulates viral replications in different species. For instance, rabbit hepatocytes had an increased *DDIT3* expression upon infection with rabbit hemorrhagic disease virus, which contributed to apoptotic liver damage (Tunon et al., 2013). Infection of porcine circovirus type 2 (PCV2) in PK-15 cells activated the PERK-eIF2 α -ATF4-*DDIT3* pathway, then deployed the UPR to enhance its replication (Zhou et al., 2016). The upregulation of *DDIT3* was also observed in HeLa cells infected with NDV, which promoted apoptosis and supported NDV proliferation (Li et al., 2019). Coxsackie virus B3 (CVB3)-induced acute viral myocarditis was associated with upregulated *DDIT3* expression in mice (Cai et al., 2015). The upregulation of *DDIT3* expression in Madin-Darby bovine kidney cells infected with bovine viral diarrhoea virus (Wang et al., 2020) and HCV-infected Huh 7 cells (Ke and Chen, 2011) was said to be involved in the regulation of innate immunity. All these studies indicated that the induced *DDIT3* upon virus infection played a role in promoting virus production.

In this study, we characterized the *DDIT3* gene in the Chinese tree shrew, a rising experimental animal for studying infectious diseases (Li et al., 2018; Xu et al., 2020b, 2020c; Yao, 2017), with an intention to learn more about the role of this gene in regulating innate immunity. We paid attention to t*DDIT3* because of an initial observation of positive selection effect in the tree shrew lineage, and we were intrigued by potential effect of the three PSSs in t*DDIT3*. Our previous studies for PSSs in MDA5 of tree shrew (Xu et al., 2016) and chicken (Xu et al., 2019a) did offer some insights into the evolutionary selection effect on immune sensors. However, we found no differences of the overexpressed t*DDIT3* mutants bearing the three PSSs on inhibiting type I IFN signaling and enhancing virus production compared to the overexpressed t*DDIT3* WT that has a stimulation effect on virus production in tree shrew cells. These results suggested that these PSSs in t*DDIT3* might be unrelated to its biological function in viral responses. Further study should be carried out to define the exact role of these PSSs in t*DDIT3* in the future. The t*DDIT3* was highly conserved compared to those of other species under study (Fig. S1) and contained the bZIP domain, which was said to be actively involved in *DDIT3*-induced apoptotic processes (Maytin et al., 2001) and acted as a key component of the enhancer-type transcription factor (Tsukano et al., 2010).

Consistent with the increased expression of h*DDIT3* upon CVB3 infection (Liu et al., 2012; Zhang et al., 2010), we found that the mRNA level of t*DDIT3* was also significantly increased in TSPRCs after HSV-1 and NDV infections. Similarly, consistent with the beneficial effects of porcine *DDIT3* and h*DDIT3* on the replication of PCV2 (Zhou et al., 2016) and infectious bronchitis virus (Liao et al., 2013), we found that overexpression of t*DDIT3* could enhance HSV-1 and VSV production in TSPRCs, whereas knockout of endogenous t*DDIT3* led to a comparable antiviral effect as that of tMAVS or tSTING overexpression. We further showed that t*DDIT3* deficiency significantly potentiated the IFN signaling as indicated by the upregulated *tIFN1* and *tISG54* mRNA expression. Concordantly, we found that overexpression of t*DDIT3* constrained the ISRE-Luc, NF- κ B-Luc and IFN- β -Luc reporter activities induced by tMDA5, tMAVS, tSTING, or tTBK1 overexpression. This observation suggested that t*DDIT3* would affect the IFN signaling pathway mediated by these immune factors, even though we found no evidence of direct interaction between t*DDIT3* and tMDA5, between t*DDIT3* and tSTING, and between t*DDIT3* and tTBK1. We speculated that the suppression effect of t*DDIT3* on luciferase activities stimulated by overexpressing tMDA5, tSTING, or tTBK1 was mediated by an unknown mechanism. Although the observed interaction between t*DDIT3* and tMAVS and ubiquitination of tMAVS in the presence of t*DDIT3* overexpression might be associated with the t*DDIT3* suppression effect on

IFN signaling stimulated by overexpressed tMAVS, we could not exclude a possibility of other potential mechanism involved in this process. Collectively, all these results indicated that the regulatory role of *DDIT3* in antiviral innate immunity was conserved in different species, and might act as a brake for balancing the upregulated antiviral innate immune responses.

The negative regulation of *DDIT3* on innate immune response is important for protecting the host against excessive IFN-induced damage (Quicke et al., 2017). Examples can be found for the binding of human oligoadenylate synthetase-like (OASL) to DNA sensor cGAS to inhibit IFN induction (Ghosh et al., 2019). Zebrafish TMEM33 acted as a negative regulator of virus-triggered IFN induction (Lu et al., 2021a). The finding of t*DDIT3* as an inhibitory regulator of MAVS-mediated signaling constituted another example in the field. More efforts should be carried out to fully uncover the underpinning of t*DDIT3*'s role in innate immunity.

One interesting observation is that t*DDIT3* had a prevalent expression in the brain tissue compared to the other tissues under physiological condition (Fig. 1C). Previous studies showed that *DDIT3* played a pivotal role in neurodegenerative diseases, as elevated expression of *DDIT3* was found in Parkinson disease (Zeng et al., 2014) and Alzheimer's disease (Baleriola et al., 2014). We speculated that the high expression of t*DDIT3* in the brain tissue might be associated with a need for monitoring potential over-activation of immune response in the brain, which is under stringent immune surveillance (Stoessel and Majewska, 2021). The exact regulatory role of t*DDIT3* in brain needs further focused examination.

In short, we characterized the role of t*DDIT3* in response to viral infections. We found that overexpression of t*DDIT3* enhanced virus infection by inhibiting the antiviral innate immune signaling, possibly via the interaction with tMAVS to enhance the ubiquitination of this important antiviral protein. A better understanding of the molecules and mechanisms that promote viral infection in the Chinese tree shrews, as exemplified by t*DDIT3*, might offer new insights into the establishment of viral infection models using this animal.

Declaration of competing interest

The authors declare no conflict of interest.

Acknowledgement

We thank Mr. Yu Li for technical assistance with the CRISPR-Cas9 editing.

Appendix A. Supplementary data

Supplementary data to this article can be found online at <https://doi.org/10.1016/j.dci.2021.104307>.

Funding

This study was supported by the National Natural Science Foundation of China (U1902215 to Y-GY), Yunnan Province (202001AS070023 to DDY), and the Chinese Academy of Sciences (Light of West China Program xbzg-zdsys-201909 to Y-GY).

References

- Amako, Y., Tsukiyama-Kohara, K., Katsume, A., Hirata, Y., Sekiguchi, S., Tobita, Y., Hayashi, Y., Hishima, T., Funata, N., Yonekawa, H., Kohara, M., 2010. Pathogenesis of hepatitis C virus infection in *Tupaia belangeri*. *J. Virol.* 84, 303–311.
- Baleriola, J., Walker, C.A., Jean, Y.Y., Crary, J.F., Troy, C.M., Nagy, P.L., Hengst, U., 2014. Axonally synthesized ATF4 transmits a neurodegenerative signal across brain regions. *Cell* 158, 1159–1172.
- Cai, Z., Shen, L., Ma, H., Yang, J., Yang, D., Chen, H., Wei, J., Lu, Q., Wang, D.W., Xiang, M., Wang, J., 2015. Involvement of endoplasmic reticulum stress-mediated C/

- EBP homologous protein activation in Coxsackievirus B3-induced acute viral myocarditis. *Circ Heart Fail* 8, 809–818.
- Che, P., Wang, M., Larson-Casey, J.L., Hu, R.H., Cheng, Y., El Hamdaoui, M., Zhao, X.K., Grytz, R., Brent Carter, A., Ding, Q., 2021. A novel tree shrew model of pulmonary fibrosis. *Lab. Invest.* 101, 116–124.
- Chen, Q., Ma, Z.X., Xia, L.B., Ye, Z.N., Liu, B.L., Ma, T.K., Bao, P.F., Wu, X.F., Yu, C.T., Ma, D.P., Han, Y.Y., Wang, W.G., Kuang, D.X., Dai, J.J., Zhang, R.P., Hu, M., Shi, H., Wang, W.L., Li, Y.J., 2020. A tree shrew model for steroid-associated osteonecrosis. *Zool. Res.* 41, 564–568.
- Fan, Y., Huang, Z.-Y., Cao, C.-C., Chen, C.-S., Chen, Y.-X., Fan, D.D., He, J., Hou, H.-L., Hu, L., Hu, X.-T., Jiang, X.-T., Lai, R., Lang, Y.-S., Liang, B., Liao, S.-G., Mu, D., Ma, Y.-Y., Niu, Y.-Y., Sun, X.-Q., Xia, J.-Q., Xiao, J., Xiong, Z.-Q., Xu, L., Yang, L., Zhang, Y., Zhao, W., Zhao, X.-D., Zheng, Y.-T., Zhou, J.-M., Zhu, Y.-B., Zhang, G.-J., Wang, J., Yao, Y.-G., 2013. Genome of the Chinese tree shrew. *Nat. Commun.* 4, 1426.
- Fan, Y., Luo, R., Su, L.-Y., Xiang, Q., Yu, D., Xu, L., Chen, J.-Q., Bi, R., Wu, D.-D., Zheng, P., Yao, Y.-G., 2018. Does the genetic feature of the Chinese tree shrew (*Tupaia belangeri chinensis*) support its potential as a viable model for Alzheimer's Disease research? *J Alzheimers Dis* 61, 1015–1028.
- Fan, Y., Ye, M.-S., Zhang, J.-Y., Xu, L., Yu, D.-D., Gu, T.-L., Yao, Y.-L., Chen, J.-Q., Lv, L.-B., Zheng, P., Wu, D.-D., Zhang, G.-J., Yao, Y.-G., 2019. Chromosomal level assembly and population sequencing of the Chinese tree shrew genome. *Zool. Res.* 40, 506–521.
- Fornace Jr., A.J., Alamo Jr., I., Hollander, M.C., 1988. DNA damage-inducible transcripts in mammalian cells. *Proc. Natl. Acad. Sci. U. S. A.* 85, 8800–8804.
- Gack, M.U., Shin, Y.C., Joo, C.H., Urano, T., Liang, C., Sun, L., Takeuchi, O., Akira, S., Chen, Z., Inoue, S., Jung, J.U., 2007. TRIM25 RING-finger E3 ubiquitin ligase is essential for RIG-I-mediated antiviral activity. *Nature* 446, 916–920.
- Ge, G.Z., Xia, H.J., He, B.L., Zhang, H.L., Liu, W.J., Shao, M., Wang, C.Y., Xiao, J., Ge, F., Li, F.B., Li, Y., Chen, C., 2016. Generation and characterization of a breast carcinoma model by PyMT overexpression in mammary epithelial cells of tree shrew, an animal close to primates in evolution. *Int. J. Cancer* 138, 642–651.
- Ghosh, A., Shao, L., Sampath, P., Zhao, B., Patel, N.V., Zhu, J., Behl, B., Parise, R.A., Beumer, J.H., O'Sullivan, R.J., DeLuca, N.A., Thorne, S.H., Rathinam, V.A.K., Li, P., Sarkar, S.N., 2019. Oligoadenylate-synthetase-family protein OASL inhibits activity of the DNA sensor cGAS during DNA virus infection to limit interferon production. *Immunity* 50, 51–63 e55.
- Gu, T., Yu, D., Fan, Y., Wu, Y., Yao, Y.-L., Xu, L., Yao, Y.-G., 2019a. Molecular identification and antiviral function of the guanylate-binding protein (GBP) genes in the Chinese tree shrew (*Tupaia belangeri chinensis*). *Dev. Comp. Immunol.* 96, 27–36.
- Gu, T., Yu, D., Li, Y., Xu, L., Yao, Y.-L., Yao, Y.-G., 2019b. Establishment and characterization of an immortalized renal cell line of the Chinese tree shrew (*Tupaia belangeri chinensis*). *Appl. Microbiol. Biotechnol.* 103, 2171–2180.
- Gu, T., Yu, D., Xu, L., Yao, Y.-L., Zheng, X., Yao, Y.-G., 2021. *Tupaia* guanylate-binding protein 1 interacts with vesicular stomatitis virus phosphoprotein and represses primary transcription of the viral genome. *Cytokine* 138, 155388.
- Guo, W.N., Zhu, B., Ai, L., Yang, D.L., Wang, B.J., 2018. Animal models for the study of hepatitis B virus infection. *Zool. Res.* 39, 25–31.
- Hu, H., Tian, M., Ding, C., Yu, S., 2018. The C/EBP homologous protein (CHOP) transcription factor functions in endoplasmic reticulum stress-induced apoptosis and microbial infection. *Front. Immunol.* 9, 3083.
- Ke, P.Y., Chen, S.S., 2011. Activation of the unfolded protein response and autophagy after hepatitis C virus infection suppresses innate antiviral immunity in vitro. *J. Clin. Invest.* 121, 37–56.
- Kock, J., Nassal, M., MacNelly, S., Baumert, T.F., Blum, H.E., von Weizsacker, F., 2001. Efficient infection of primary tupaia hepatocytes with purified human and woolly monkey hepatitis B virus. *J. Virol.* 75, 5084–5089.
- Kumar, S., Stecher, G., Tamura, K., 2016. MEGA7: molecular evolutionary genetics analysis version 7.0 for bigger datasets. *Mol. Biol. Evol.* 33, 1870–1874.
- Li, H., Liu, B., Lian, L., Zhou, J., Xiang, S., Zhai, Y., Chen, Y., Ma, X., Wu, H., Hou, L., 2021. High dose expression of heme oxygenase-1 induces renal degeneration through ER stress-related DDIT3. *Mol. Neurodegener.* 16, 16.
- Li, L., Li, Z., Wang, E., Yang, R., Xiao, Y., Han, H., Lang, F., Li, X., Xia, Y., Gao, F., Li, Q., Fraser, N.W., Zhou, J., 2016. Herpes simplex virus 1 infection of tree shrews differs from that of mice in the severity of acute infection and viral transcription in the peripheral nervous system. *J. Virol.* 90, 790–804.
- Li, R., Zanin, M., Xia, X., Yang, Z., 2018. The tree shrew as a model for infectious diseases research. *J. Thorac. Dis.* 10, S2272–S2279.
- Li, Y., Jiang, W., Niu, Q., Sun, Y., Meng, C., Tan, L., Song, C., Qiu, X., Liao, Y., Ding, C., 2019. eIF2alpha-CHOP-BCL-2/JNK and IRE1alpha-XBP1/JNK signaling promote apoptosis and inflammation and support the proliferation of Newcastle disease virus. *Cell Death Dis.* 10, 891.
- Liao, Y., Fung, T.S., Huang, M., Fang, S.G., Zhong, Y., Liu, D.X., 2013. Upregulation of CHOP/GADD153 during coronavirus infectious bronchitis virus infection modulates apoptosis by restricting activation of the extracellular signal-regulated kinase pathway. *J. Virol.* 87, 8124–8134.
- Liu, Z., Zhang, H.M., Yuan, J., Ye, X., Taylor, G.A., Yang, D., 2012. The immunity-related GTPase Irgm3 relieves endoplasmic reticulum stress response during coxsackievirus B3 infection via a PI3K/Akt dependent pathway. *Cell Microbiol.* 14, 133–146.
- Lu, L.F., Zhang, C., Li, Z.C., Zhou, X.Y., Jiang, J.Y., Chen, D.D., Zhang, Y.A., Xiong, F., Zhou, F., Li, S., 2021a. A novel role of Zebrafish TMEM33 in negative regulation of interferon production by two distinct mechanisms. *PLoS Pathog.* 17, e1009317.
- Lu, T., Peng, H., Zhong, L., Wu, P., He, J., Deng, Z., Huang, Y., 2021b. The tree shrew as a model for cancer research. *Front Oncol* 11, 653236.
- Luo, M.-T., Mu, D., Yang, X., Luo, R.-H., Zheng, H.-Y., Chen, M., Guo, Y.-Q., Zheng, Y.-T., 2021. Tree shrew cells transduced with human CD4 and CCR5 support early Steps of HIV-1 replication, but viral infectivity is restricted by APOBEC3. *J. Virol.* 95, e0002021.
- Luo, M.-T., Zheng, Y.-T., 2020. The tsAPOBEC3 proteins restrict HBV replication and may limit the establishment of persistent infection in tree shrews. *Cell. Mol. Immunol.* 17, 1107–1108.
- Ma, X., Wong, A.-S., Tam, H.-Y., Tsui, S.-Y., Chung, D.L., Feng, B., 2018. In vivo genome editing thrives with diversified CRISPR technologies. *Zool. Res.* 39, 58–71.
- Maytin, E.V., Ubeda, M., Lin, J.C., Habener, J.F., 2001. Stress-inducible transcription factor CHOP/gadd153 induces apoptosis in mammalian cells via p38 kinase-dependent and -independent mechanisms. *Exp. Cell Res.* 267, 193–204.
- Medigeshi, G.R., Lancaster, A.M., Hirsch, A.J., Briese, T., Lipkin, W.I., DeFilippis, V., Fruh, K., Mason, P.W., Nikolich-Zugich, J., Nelson, J.A., 2007. West Nile virus infection activates the unfolded protein response, leading to CHOP induction and apoptosis. *J. Virol.* 81, 10849–10860.
- Oliveros, J.C., Franch, M., Tabas-Madrid, D., San-Leon, D., Montoliu, L., Cubas, P., Pazos, F., 2016. Breaking-Cas-interactive design of guide RNAs for CRISPR-Cas experiments for ENSEMBL genomes. *Nucleic Acids Res.* 44, W267–W271.
- Oyadomari, S., Mori, M., 2004. Roles of CHOP/GADD153 in endoplasmic reticulum stress. *Cell Death Differ.* 11, 381–389.
- Peng, Y., Ye, Z., Zou, R., Wang, Y., Tian, B., Ma, Y., Shi, L., 1991. Biology of Chinese Tree Shrews (*Tupaia Belangeri Chinensis*). Yunnan Science and Technology Press, Kunming, China.
- Pennuto, M., Tinelli, E., Malaguti, M., Del Carro, U., D'Antonio, M., Ron, D., Quattrini, A., Feltri, M.L., Wrabetz, L., 2008. Ablation of the UPR-mediator CHOP restores motor function and reduces demyelination in Charcot-Marie-Tooth 1B mice. *Neuron* 57, 393–405.
- Quicke, K.M., Diamond, M.S., Suthar, M.S., 2017. Negative regulators of the RIG-I-like receptor signaling pathway. *Eur. J. Immunol.* 47, 615–628.
- Ran, F.A., Hsu, P.D., Wright, J., Agarwala, V., Scott, D.A., Zhang, F., 2013. Genome engineering using the CRISPR-Cas9 system. *Nat. Protoc.* 8, 2281–2308.
- Ron, D., Habener, J.F., 1992. CHOP, a novel developmentally regulated nuclear protein that dimerizes with transcription factors C/EBP and LAP and functions as a dominant-negative inhibitor of gene transcription. *Genes Dev.* 6, 439–453.
- Rouschop, K.M., van den Beucken, T., Dubois, L., Niessen, H., Bussink, J., Savelkoul, K., Keulers, T., Mujic, H., Landuyt, W., Voncken, J.W., Lambin, P., van der Kogel, A.J., Koritzinsky, M., Wouters, B.G., 2010. The unfolded protein response protects human tumor cells during hypoxia through regulation of the autophagy genes MAP1LC3B and ATG5. *J. Clin. Invest.* 120, 127–141.
- Savner, E., Sedigh-Sarvestani, M., Wimmer, R., Fitzpatrick, D., 2021. A bright future for the tree shrew in neuroscience research: summary from the inaugural tree shrew users meeting. *Zool. Res.* 42, 478–481.
- Stoessel, M.B., Majewska, A.K., 2021. Little cells of the little brain: microglia in cerebellar development and function. *Trends Neurosci.* 44, 564–578.
- Sun, J., Liu, W., Guo, Y., Zhang, H., Jiang, D., Luo, Y., Liu, R., Chen, C., 2021. Characterization of tree shrew telomeres and telomerase. *J. Genet. Genomics* 48, 631–639.
- Tsukada, J., Yoshida, Y., Kominato, Y., Auron, P.E., 2011. The CCAAT/enhancer (C/EBP) family of basic-leucine zipper (bZIP) transcription factors is a multifaceted highly-regulated system for gene regulation. *Cytokine* 54, 6–19.
- Tsukano, H., Gotoh, T., Endo, M., Miyata, K., Tazume, H., Kadomatsu, T., Yano, M., Iwakaki, T., Kohno, K., Araki, K., Mizuta, H., Oike, Y., 2010. The endoplasmic reticulum stress-C/EBP homologous protein pathway-mediated apoptosis in macrophages contributes to the instability of atherosclerotic plaques. *Arterioscler. Thromb. Vasc. Biol.* 30, 1925–1932.
- Tunon, M.J., San-Miguel, B., Crespo, I., Laliena, A., Vallejo, D., Alvarez, M., Prieto, J., Gonzalez-Gallego, J., 2013. Melatonin treatment reduces endoplasmic reticulum stress and modulates the unfolded protein response in rabbits with lethal fulminant hepatitis of viral origin. *J. Pineal Res.* 55, 221–228.
- Ubeda, M., Wang, X.Z., Zinsner, H., Wu, I., Habener, J.F., Ron, D., 1996. Stress-induced binding of the transcriptional factor CHOP to a novel DNA control element. *Mol. Cell Biol.* 16, 1479–1489.
- Versteeg, G.A., Rajsbaum, R., Sanchez-Aparicio, M.T., Maestre, A.M., Valdiviezo, J., Shi, M., Inn, K.S., Fernandez-Sesma, A., Jung, J., Garcia-Sastre, A., 2013. The E3-ligase TRIM family of proteins regulates signaling pathways triggered by innate immune pattern-recognition receptors. *Immunity* 38, 384–398.
- Wang, S., Hou, P., Pan, W., He, W., He, D.C., Wang, H., He, H., 2020. DDIT3 targets innate immunity via the DDIT3-OTUD1-MAVS pathway to promote BVDV replication. *J. Virol.* 95, e02320, 02351.
- Xiao, J., Liu, R., Chen, C.-S., 2017. Tree shrew (*Tupaia belangeri*) as a novel laboratory disease animal model. *Zool. Res.* 38, 127–137.
- Xu, L., Yu, D.-D., Ma, Y.-H., Yao, Y.-L., Luo, R.-H., Feng, X.-L., Cai, H.-R., Han, J.-B., Wang, X.-H., Li, M.-H., Ke, C.-W., Zheng, Y.-T., Yao, Y.-G., 2020a. COVID-19-like symptoms observed in Chinese tree shrews infected with SARS-CoV-2. *Zool. Res.* 41, 517–526.
- Xu, L., Yu, D., Fan, Y., Liu, Y.-P., Yao, Y.-G., 2019a. Evolutionary selection on MDA5 and LGP2 in the chicken preserves antiviral competence in the absence of RIG-I. *J. Genet. Genomics* 46, 499–503.
- Xu, L., Yu, D., Fan, Y., Peng, L., Wu, Y., Yao, Y.-G., 2016. Loss of RIG-I leads to a functional replacement with MDA5 in the Chinese tree shrew. *Proc. Natl. Acad. Sci. U. S. A.* 113, 10950–10955.
- Xu, L., Yu, D., Peng, L., Fan, Y., Chen, J., Zheng, Y.-T., Wang, C., Yao, Y.-G., 2015. Characterization of a MAVS ortholog from the Chinese tree shrew (*Tupaia belangeri chinensis*). *Dev. Comp. Immunol.* 52, 58–68.
- Xu, L., Yu, D., Peng, L., Wu, Y., Fan, Y., Gu, T., Yao, Y.-L., Zhong, J., Chen, X., Yao, Y.-G., 2020b. An alternative splicing of *tupaia* STING modulated anti-RNA virus responses by targeting MDA5-LGP2 and IRF3. *J. Immunol.* 204, 3191–3204.

- Xu, L., Yu, D., Yao, Y.-L., Gu, T., Zheng, X., Wu, Y., Luo, R.-H., Zheng, Y.-T., Zhong, J., Yao, Y.-G., 2020c. *Tupaia* MAVS is a dual target during hepatitis C virus infection for innate immune evasion and viral replication via NF- κ B. *J. Immunol.* 205, 2091–2099.
- Xu, S., Li, X., Yang, J., Wang, Z., Jia, Y., Han, L., Wang, L., Zhu, Q., 2019b. Comparative pathogenicity and transmissibility of pandemic H1N1, avian H5N1, and human H7N9 influenza viruses in tree shrews. *Front. Microbiol.* 10, 2955.
- Xu, X., Chen, H., Cao, X., Ben, K., 2007. Efficient infection of tree shrew (*Tupaia belangeri*) with hepatitis C virus grown in cell culture or from patient plasma. *J. Gen. Virol.* 88, 2504–2512.
- Yang, Y., Liu, L., Naik, I., Braunstein, Z., Zhong, J., Ren, B., 2017. Transcription factor C/EBP homologous protein in health and diseases. *Front. Immunol.* 8, 1612.
- Yang, Z., 2007. PAML 4: phylogenetic analysis by maximum likelihood. *Mol. Biol. Evol.* 24, 1586–1591.
- Yang, Z., Nielsen, R., 2002. Codon-substitution models for detecting molecular adaptation at individual sites along specific lineages. *Mol. Biol. Evol.* 19, 908–917.
- Yang, Z., Wong, W.S., Nielsen, R., 2005. Bayes empirical bayes inference of amino acid sites under positive selection. *Mol. Biol. Evol.* 22, 1107–1118.
- Yang, Z.F., Zhao, J., Zhu, Y.T., Wang, Y.T., Liu, R., Zhao, S.S., Li, R.F., Yang, C.G., Li, J. Q., Zhong, N.S., 2013. The tree shrew provides a useful alternative model for the study of influenza H1N1 virus. *Virol. J.* 10, 111.
- Yao, Y.-G., 2017. Creating animal models, why not use the Chinese tree shrew (*Tupaia belangeri chinensis*)? *Zool. Res.* 38, 118–126.
- Yao, Y.-L., Yu, D., Xu, L., Fan, Y., Wu, Y., Gu, T., Chen, J., Lv, L.B., Yao, Y.-G., 2019. Molecular characterization of the 2',5'-oligoadenylate synthetase family in the Chinese tree shrew (*Tupaia belangeri chinensis*). *Cytokine* 114, 106–114.
- Yao, Y.-L., Yu, D., Xu, L., Gu, T., Li, Y., Zheng, X., Bi, R., Yao, Y.-G., 2020. *Tupaia* OASL1 promotes cellular antiviral immune responses by recruiting MDA5 to MAVS. *J. Immunol.* 205, 3419–3428.
- Ye, M.S., Zhang, J.Y., Yu, D.D., Xu, M., Xu, L., Lv, L.B., Zhu, Q.Y., Fan, Y., Yao, Y.-G., 2021. Comprehensive annotation of the Chinese tree shrew genome by large-scale RNA sequencing and long-read isoform sequencing. *Zool. Res.* 42, 692–709.
- Yin, C., Zhou, X., Yao, Y.-G., Wang, W., Wu, Q., Wang, X., 2020. Abundant self-amplifying intermediate progenitors in the subventricular zone of the Chinese tree shrew neocortex. *Cerebr. Cortex* 30, 3370–3380.
- Yong, J., Parekh, V.S., Reilly, S.M., Nayak, J., Chen, Z., Lebeaupin, C., Jang, I., Zhang, J., Prakash, T.P., Sun, H., Murray, S., Guo, S., Ayala, J.E., Satin, L.S., Saltiel, A.R., Kaufman, R.J., 2021. Chop/Ddit3 depletion in beta cells alleviates ER stress and corrects hepatic steatosis in mice. *Sci. Transl. Med.* 13, e9796.
- Yu, D., Wu, Y., Xu, L., Fan, Y., Peng, L., Xu, M., Yao, Y.-G., 2016. Identification and characterization of toll-like receptors (TLRs) in the Chinese tree shrew (*Tupaia belangeri chinensis*). *Dev. Comp. Immunol.* 60, 127–138.
- Yu, D., Xu, L., Liu, X.-H., Fan, Y., Lu, L.-B., Yao, Y.-G., 2014. Diverse interleukin-7 mRNA transcripts in Chinese tree shrew (*Tupaia belangeri chinensis*). *PLoS One* 9, e99859.
- Zeng, X.-S., Jia, J.-J., Kwon, Y., Wang, S.-D., Bai, J., 2014. The role of thioredoxin-1 in suppression of endoplasmic reticulum stress in Parkinson disease. *Free Radic. Biol. Med.* 67, 10–18.
- Zhang, H.M., Ye, X., Su, Y., Yuan, J., Liu, Z., Stein, D.A., Yang, D., 2010. Coxsackievirus B3 infection activates the unfolded protein response and induces apoptosis through downregulation of p58IPK and activation of CHOP and SREBP1. *J. Virol.* 84, 8446–8459.
- Zhang, J., Luo, R.-C., Man, X.-Y., Lv, L.-B., Yao, Y.-G., Zheng, M., 2020a. The anatomy of the skin of the Chinese tree shrew is very similar to that of human skin. *Zool. Res.* 41, 208–212.
- Zhang, J., Nielsen, R., Yang, Z., 2005. Evaluation of an improved branch-site likelihood method for detecting positive selection at the molecular level. *Mol. Biol. Evol.* 22, 2472–2479.
- Zhang, L., Shen, Z.L., Feng, Y., Li, D.Q., Zhang, N.N., Deng, Y.Q., Qi, X.P., Sun, X.M., Dai, J.J., Yang, C.G., Yang, Z.F., Qin, C.F., Xia, X.S., 2019. Infectivity of Zika virus on primary cells support tree shrew as animal model. *Emerg. Microb. Infect.* 8, 232–241.
- Zhang, M., Guo, Y., Fu, H., Hu, S., Pan, J., Wang, Y., Cheng, J., Song, J., Yu, Q., Zhang, S., Xu, J.F., Pei, G., Xiang, X., Yang, P., Wang, C.Y., 2015. Chop deficiency prevents UUU-induced renal fibrosis by attenuating fibrotic signals originated from Hmgb1/TLR4/NF κ B/IL-1 β signaling. *Cell Death Dis.* 6, e1847.
- Zhang, X., Yu, D., Wu, Y., Gu, T., Ma, N., Dong, S., Yao, Y.-G., 2020b. Establishment and transcriptomic features of an immortalized hepatic cell line of the Chinese tree shrew. *Appl. Microbiol. Biotechnol.* 104, 8813–8823.
- Zheng, Y., Gao, C., 2020. Fine-tuning of antiviral innate immunity by ubiquitination. *Adv. Immunol.* 145, 95–128.
- Zhou, Y., Qi, B., Gu, Y., Xu, F., Du, H., Li, X., Fang, W., 2016. Porcine circovirus 2 deploys PERK pathway and GRP78 for its enhanced replication in PK-15 cells. *Viruses* 8, 56.

Table S1. Primer pairs used in this study

Primer name	Primer sequence (5' - 3')	Application and vector
tDDIT3-FLAG F	CGgatccATGGCAGCTGAGTCATTGCC	PCR for constructing tDDIT3 expression vector (tDDIT3-FLAG) using the pCMV-3Tag-8 vector
tDDIT3-FLAG R	CCGctcgagGCTTTGGTGCAGATTAACCA	
tDDIT3-HA F	GgaattcggATGGCAGCTGAGTCATTGCC	PCR for constructing tDDIT3 expression vector (tDDIT3-HA) using the pCMV-HA vector
tDDIT3-HA R	CCGctcgagtcGCTTTGGTGCAGATTAA	
tDDIT3-RT-qPCR F	GGAAAGCAGCGCATGAAG	Quantitative real-time PCR (qRT-PCR) for quantification of <i>tDDIT3</i> mRNA level
tDDIT3-RT-qPCR R	TTCGGTCAATCAGAGCTCGG	
tDDIT3-sgRNA F	CACCGCCAGCTGGACAGTGTCCCGA	Constructing the CRISPR/Cas9 vector for tDDIT3 knockout using the pX330-T7 vector
tDDIT3-sgRNA R	AAACTCGGGACACTGTCCAGCTGGC	
p.E83D	TTGTTCTCCGGATTCCAGTCAGAGTTC GAACTCTGACTGGAAATCCGGAGAACAA	PCR to introduce a change of glutamic acid (E) to aspartic acid (D) at the 83 rd position in tDDIT3 using the tDDIT3-FLAG vector
p.S172A	ATCTGCACCAAGCCCTCGAGGATTACA TGTAATCCTCGAGGGCTTGGTGCAGAT	PCR to introduce a change of serine (S) to alanine (A) at the 172 nd position in tDDIT3 using the tDDIT3-FLAG vector
p.S89_S92 del	TGTTCTCCGGAATCCAGTCAGAGTCCCCGGCTCAGGAG CTCCTGAGCCGGGAACTCTGACTGGATTCCGGAGAACA	PCR to introduce a deletion of the Serine-Glutamine-Serine-Serine (SQSS) repeat in tDDIT3 using the tDDIT3-FLAG vector
tIFNB1-F	ACCACTTGAAAACCATGC	qRT-PCR for quantification of <i>tIFNB1</i> mRNA level. The primer pair was taken from Yao et al. (2020)
tIFNB1-R	TTTCCACTCGGACTATCG	
tISG54-F	CTATCTGTATTGCCGTATTGG	qRT-PCR for quantification of <i>tISG54</i> mRNA level. The primer pair was taken from Yao et al. (2020)
tISG54-R	CTTCTGTCTCTCCTCTG	
tTRIM 25-FLAG F	ACgatataATGGCGGAGCTGGGCCACC	PCR for constructing tTRIM 25 expression vector (tTRIM25-FLAG) using the pCMV-3Tag-8 vector
tTRIM 25-FLAG R	ATctcgagATACTTGGGGGGGCAGATG	

The nucleotides in the lowercase stand for the site of restricted enzyme. The nucleotides in italic were for introducing point mutations. For the numbering of the residue changes in tDDIT3, please refer to the aligned DDIT3 protein sequences in Figure S1.

Table S2. Accession numbers of the *DDIT3* gene from twelve mammalian species used for the phylogenetic analysis

Species	Accession number in ESMBL ^a
<i>Homo sapiens</i>	ENST00000551116.5
<i>Pan troglodytes</i>	ENSPTRT00000047450.5
<i>Gorilla gorilla gorilla</i>	ENSGGOT00000001997.3
<i>Canis lupus familiaris</i>	ENSCAFT00000047972.2
<i>Macaca mulatta</i>	ENSMMUT00000107307.1
<i>Tupaia belangeri chinensis</i>	OK076936 ^b
<i>Mus musculus</i>	ENSMUST00000026475.14
<i>Rattus norvegicus</i>	ENSRNOT00000083472.1
<i>Bos taurus</i>	ENSBTAT00000044712.2
<i>Oryctolagus cuniculus</i>	ENSOCUT00000024134.1
<i>Ochotona princeps</i>	ENSOPRT00000006522.1
<i>Loxodonta africana</i>	ENSLAFT00000029487.1

^a ENSEMBL (<http://www.ensembl.org/index.html>)

^b This GenBank sequence can be retrieved from www.treeshrewdb.org by accession number TSDBT00030502.1.

Tupaia belangeri chinensis : MAAEELPFSEFGLSSWELEAWYIDLQEVLSSENGGTYVSPFNKEEESKIFTTFLDPAS : 59
Homo sapiens : MAAEELPFSEFGLSSWELEAWYIDLQEVLSSENGGTYVSPFNKEEESKIFTTFLDPAS : 59
Mus musculus : MAAEELPFSEFGLSSWELEAWYIDLQEVLSSENGGTYVSPFNKEEESKIFTTFLDPAS : 59
Rattus norvegicus : MAAEELPFSEFGLSSWELEAWYIDLQEVLSSENGGTYVSPFNKEEESKIFTTFLDPAS : 59
Macaca mulatta : MAAEELPFSEFGLSSWELEAWYIDLQEVLSSENGGTYVSPFNKEEESKIFTTFLDPAS : 59
Gorilla gorilla gorilla : MAAEELPFSEFGLSSWELEAWYIDLQEVLSSENGGTYVSPFNKEEESKIFTTFLDPAS : 59
Pan troglodytes : MAAEELPFSEFGLSSWELEAWYIDLQEVLSSENGGTYVSPFNKEEESKIFTTFLDPAS : 59
Canis lupus familiaris : MAAEELPFSEFGLSSWELEAWYIDLQEVLSSENGGTYVSPFNKEEESKIFTTFLDPAS : 59
Oryctolagus cuniculus : MAAEELPFSEFGLSSWELEAWYIDLQEVLSSENGGTYVSPFNKEEESKIFTTFLDPAS : 59
Ochotona princeps : MAAEELPFSEFGLSSWELEAWYIDLQEVLSSENGGTYVSPFNKEEESKIFTTFLDPAS : 59
Bos taurus : MAAEELPFSEFGLSSWELEAWYIDLQEVLSSENGGTYVSPFNKEEESKIFTTFLDPAS : 59
Loxodonta africana : MAAEELPFSEFGLSSWELEAWYIDLQEVLSSENGGTYVSPFNKEEESKIFTTFLDPAS : 59

bZIP

Tupaia belangeri chinensis : LAWLLEEFGPEVTSSTSCSPSPSSSSSQSSPAQEEEEEDQGRTRKRKQSGQSPAR : 117
Homo sapiens : LAWLLEEFGPEVTSSTSCSPSPSSSSSQSSPAQEEEEEDQGRTRKRKQSGHSPAR : 114
Mus musculus : LAWLLEEFGPEVTSSTSCSPSPSSSSSQSSPAQEEEEEDQGRTRKRKQSGQCPAR : 113
Rattus norvegicus : LAWLLEEFGPEVTSSTSCSPSPSSSSSQSSPAQEEEEEDQGRTRKRKQSGQCPAR : 113
Macaca mulatta : LAWLLEEFGPEVTSSTSCSPSPSSSSSQSSPAQEEEEEDQGRTRKRKQSGHSPAR : 114
Gorilla gorilla gorilla : LAWLLEEFGPEVTSSTSCSPSPSSSSSQSSPAQEEEEEDQGRTRKRKQSGHSPAR : 114
Pan troglodytes : LAWLLEEFGPEVTSSTSCSPSPSSSSSQSSPAQEEEEEDQGRTRKRKQSGHSPAR : 114
Canis lupus familiaris : LAWLLEEFGPEVTSSTSCSPSPSSSSSQSSPAQEEEEEDQGRTRKRKQSGQCPAR : 113
Oryctolagus cuniculus : LAWLLEEFGPEVTSSTSCSPSPSSSSSQSSPAQEEEEEDQGRTRKRKQSGQCPAR : 113
Ochotona princeps : LAWLLEEFGPEVTSSTSCSPSPSSSSSQSSPAQEEEEEDQGRTRKRKQSGQSPAR : 112
Bos taurus : LAWLLEEFGPEVTSSTSCSPSPSSSSSQSSPAQEEEEEDQGRTRKRKQSGQSPAR : 113
Loxodonta africana : LAWLLEEFGPEVTSSTSCSPSPSSSSSQSSPAQEEEEEDQGRTRKRKQSGQSPAR : 113

bZIP

Tupaia belangeri chinensis : AGKQRMKEKEQENERKVAQLAEENRLKQIEELTREVEATRRALIDRMVNLHQAS* : 172
Homo sapiens : AGKQRMKEKEQENERKVAQLAEENRLKQIEELTREVEATRRALIDRMVNLHQAA* : 169
Mus musculus : AGKQRMKEKEQENERKVAQLAEENRLKQIEELTREVEATRRALIDRMVNLHQAA* : 168
Rattus norvegicus : AGKQRMKEKEQENERKVAQLAEENRLKQIEELTREVEATRRALIDRMVNLHQAA* : 168
Macaca mulatta : AGKQRMKEKEQENERKVAQLAEENRLKQIEELTREVEATRRALIDRMVNLHQAA* : 169
Gorilla gorilla gorilla : AGKQRMKEKEQENERKVAQLAEENRLKQIEELTREVEATRRALIDRMVNLHQAA* : 169
Pan troglodytes : AGKQRMKEKEQENERKVAQLAEENRLKQIEELTREVEATRRALIDRMVNLHQAA* : 169
Canis lupus familiaris : AGKQRMKEKEQENERKVAQLAEENRLKQIEELTREVEATRRALIDRMVNLHQAA* : 168
Oryctolagus cuniculus : AGKQRMKEKEQENERKVAQLAEENRLKQIEELTREVEATRRALIDRMVNLHQAA* : 168
Ochotona princeps : AGKQRMKEKEQENERKVAQLAEENRLKQIEELTREVEATRRALIDRMVNLHQAA* : 167
Bos taurus : AGKQRMKEKEQENERKVAQLAEENRLKQIEELTREVEATRRALIDRMVNLHQAA* : 168
Loxodonta africana : AGKQRMKEKEQENERKVAQLAEENRLKQIEELTREVEATRRALIDRMVNLHQAA* : 168

Figure S1. Alignment of the DDIT3 protein sequences in the Chinese tree shrew and several mammals. The accession numbers for the related species were listed in Table S2. The three positively selected sites in tDDIT3 were marked by * in the aligned sequences. The basic-leucine zipper (bZIP) motif was in red box.

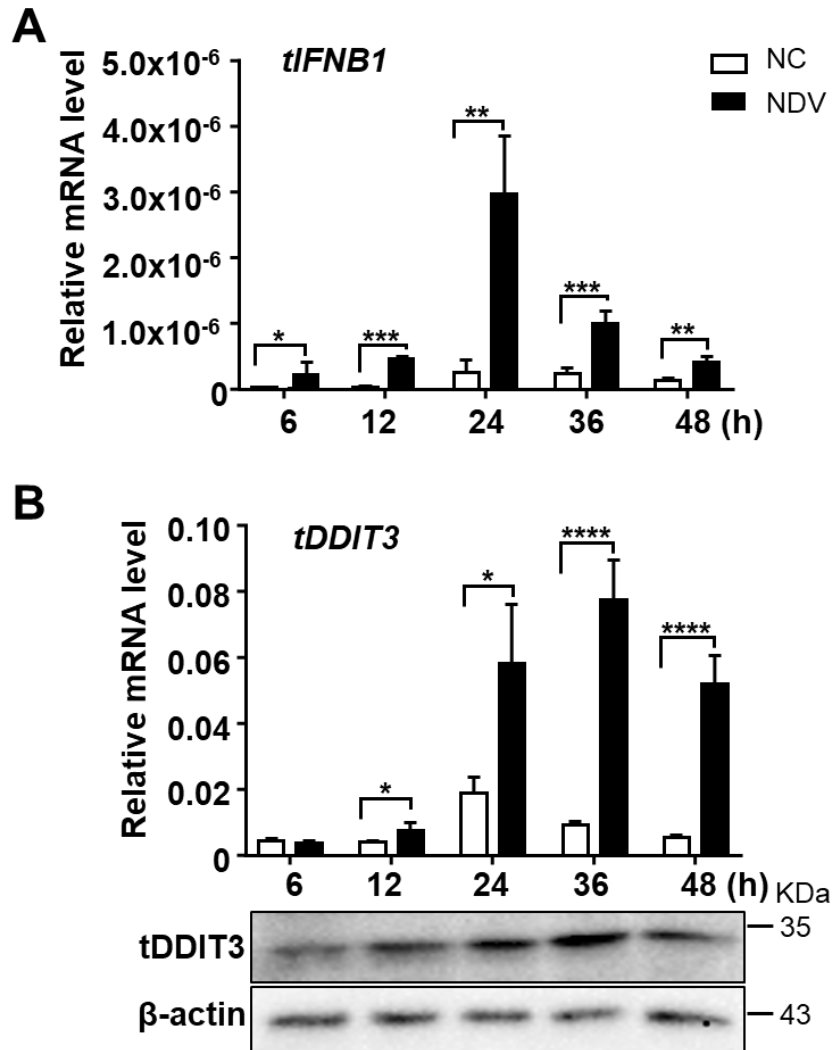


Figure S2. Virus infection upregulated *tDDIT3* expression in a time dependent manner. TSPRCs (5×10^4 cells) were seeded in 24-well plates for overnight growth, followed by NDV infection (MOI=1) or being uninfected (NC). Cells were harvested to quantify the relative mRNA levels of *tIFNB1* (A) and *tDDIT3* (B) at the indicated times, following the same procedure as in Figure 1E. Western blot for *tDDIT3* and β -actin was shown in the below panel of (B). The TSPRCs in this assay was from a different animal compared to those TSPRCs used in Figure 1E. Values of relative mRNA levels of *tDDIT3* were presented as mean \pm SD. * $P < 0.05$, ** $P < 0.01$, *** $P < 0.001$, **** $P < 0.0001$, two-tailed unpaired Student's *t*-test.

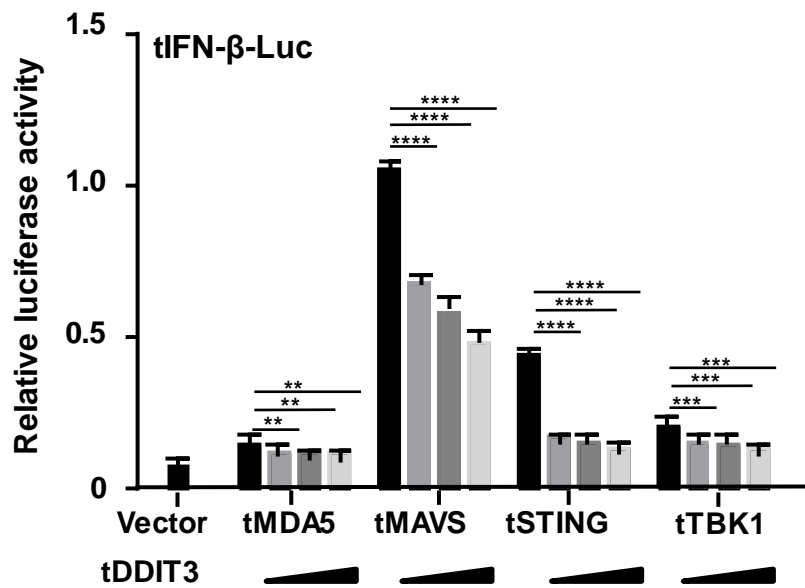


Figure S3. Overexpression of tDDIT3 reduced the tree shrew IFN- β -Luc reporter luciferase activity stimulated by overexpressed tMDA5, tMAVS, tSTING or tTBK1 in a dose-dependent manner. HEK293T cells (5×10^4 cells) were transfected with an increased amount (0 ng, 150 ng, 300 ng, and 600 ng) of tDDIT3 expression vector (with empty vector to reach a total amount of 600 ng), expression vector of immune factor (tMDA5-HA, tMAVS-HA, tSTING-Myc, or tTBK1-FLAG; each 300 ng), together with tree shrew IFN- β -Luc reporter vector (100ng) and TK (10 ng, as an inner control).